RTI PAST PERFORMANCE	
RTI Tracking Number:	1312938 Date 2/4/2014
Core Task:	Mechanical Testing, Metallurgical Testing, Fatigue Failure Testing
Analytical Techniques	Mechanical/Hardness/ Feature/Microhardness/photo/SEM/EDS

A motor assembly with a shaft failure was received for analysis. The target of the analysis was to investigate the failure mode and materials properties using a variety of metallographic techniques. The results of the analysis are discussed below.

Visual Observation and Fractography:
A complete wrapped motor assembly was received in the laboratory. Upon removal of the wrapping material, a large crack was noted circuferentially around the shaft at the reduced section machining radius. The shaft and features were photodocumented as below, with the initial crack at the 0 deg position, and the 3 other quadrants identified clockwise in the crack propagation direction.

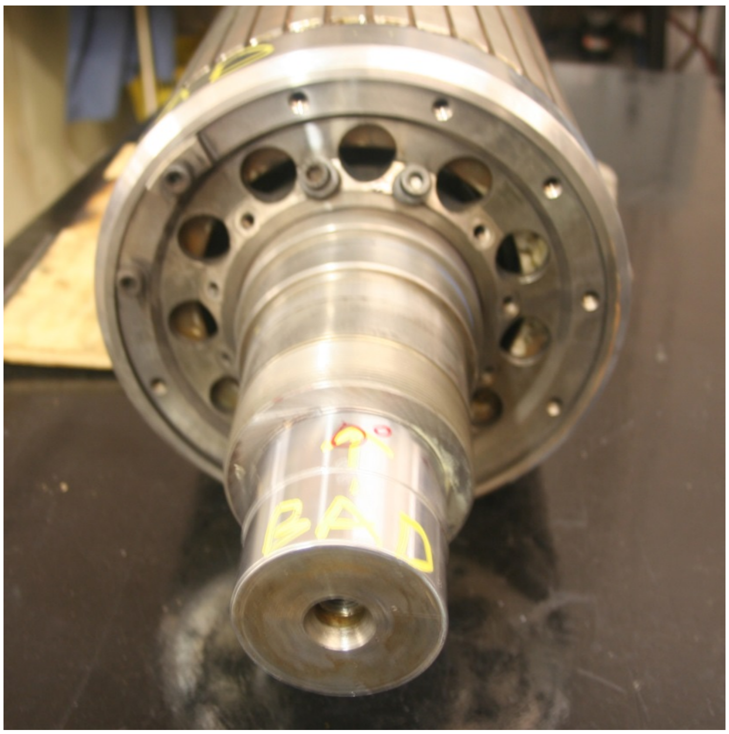

Figure 1 – As received motor and exposed shaft

Figure 2 – 0 degree and crack origin

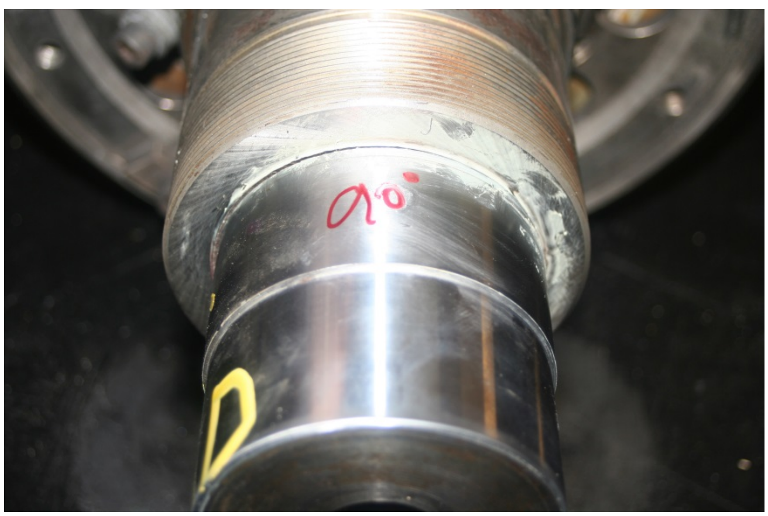

Figure 3 – 90 degree crack propagation

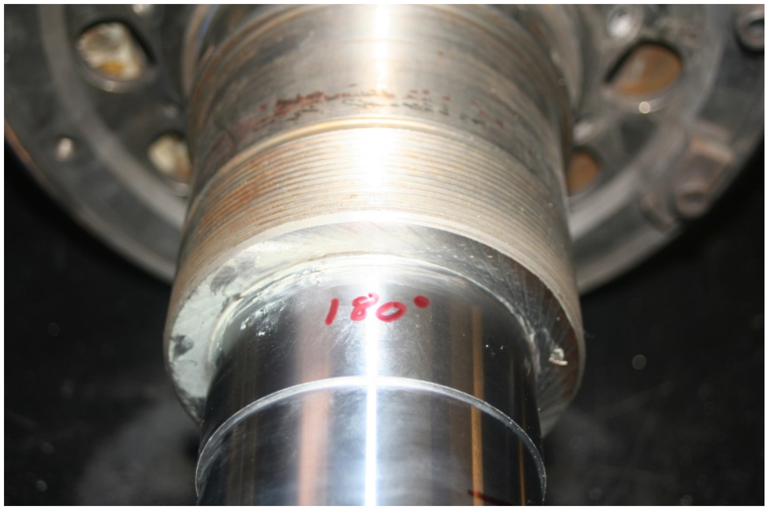

Figure 4 – 180 deg crack propagation

Figure 5 – 270 degree crack propagation

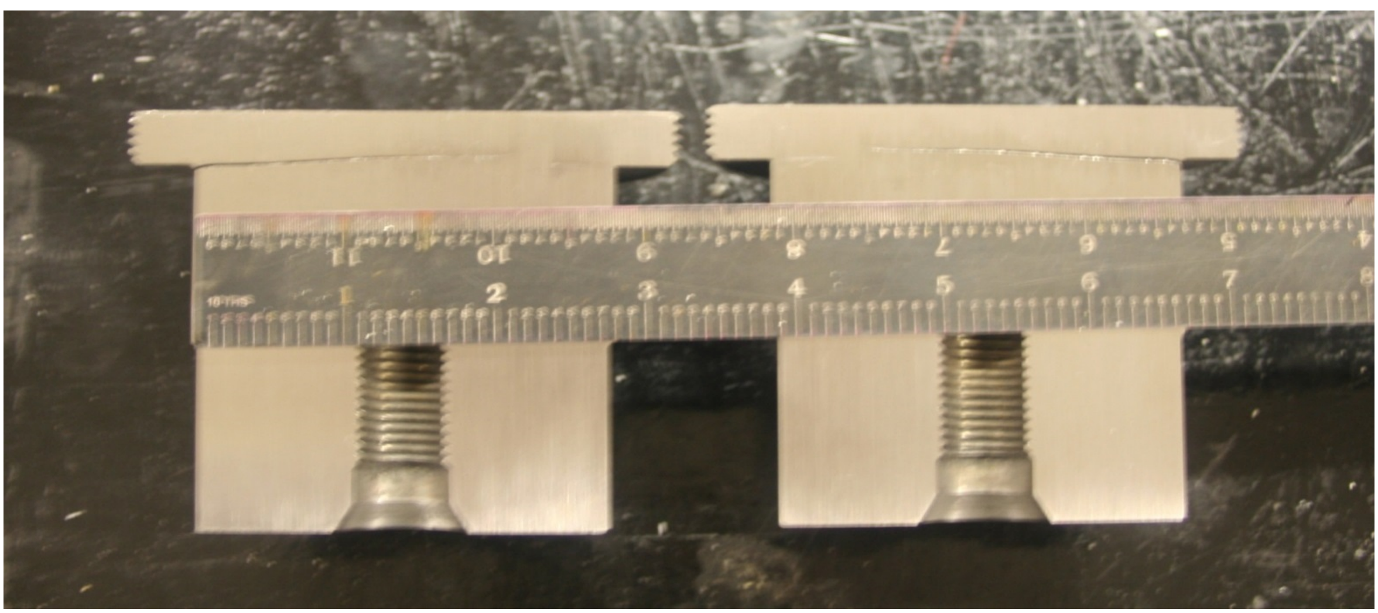

Figure 6 – Longitudinal cut of the isolated shaft crack region

The fracture region was isolated from the bulk shaft and further sectioned longitudinal to detail the crack propagation in the profile view. The image shows the propagation past the center point, with a minor crack also evident on the opposite side meeting at the plane of retained metal.

A further longitudinal cut was made through the crack zone to "open up" the crack region to examine the bulk fracture morphology. The images below detail the fracture morphology in 3 regions as described.

Figure 7 – Photomicrograph obtained from fracture area A at 7X magnification

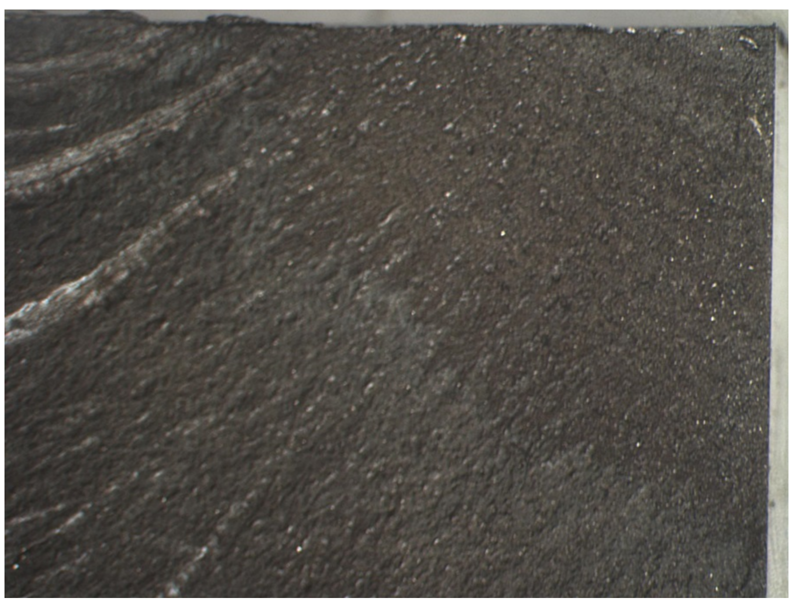

Figure 8 – Photomicrograph obtained from area B at 7X magnification

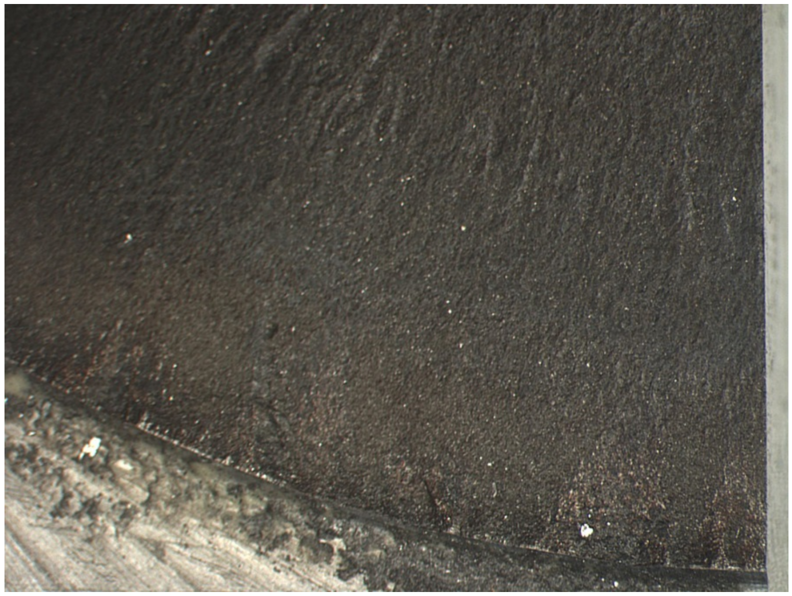

Figure 9 – Photomicrograph obtained from area C at 7X magnification

The fracture section was cleaned of oxidation and the morphology of the fracture imaged by SEM (Scanning Electron Microscopy) to observe any micro-features of the fracture morphology contributing to the failure mode. The resulting SEM images are provided below.

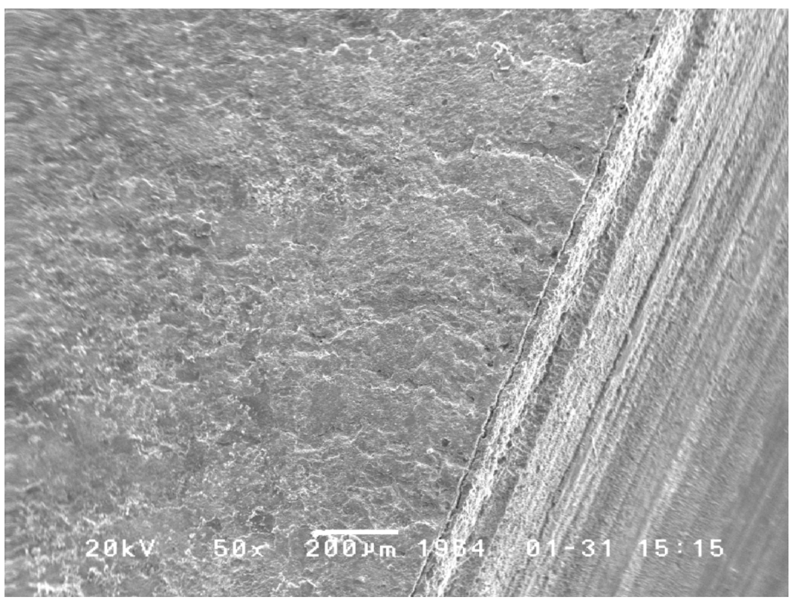

Figure 10 – SEM photomicrograph obtained at 50X magnification at the circumference area

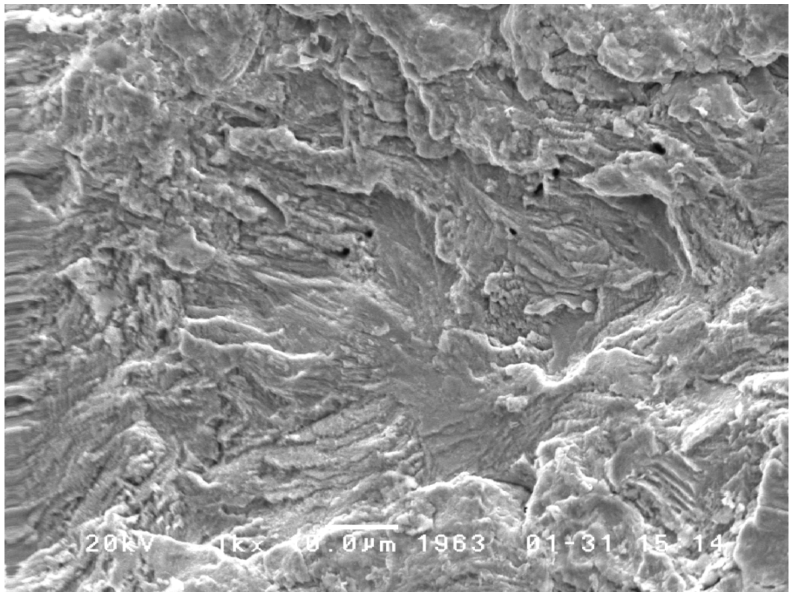

Figure 11 – SEM photomicrograph obtained at 1000X magnification at the circumference area indicating cleavage morphology

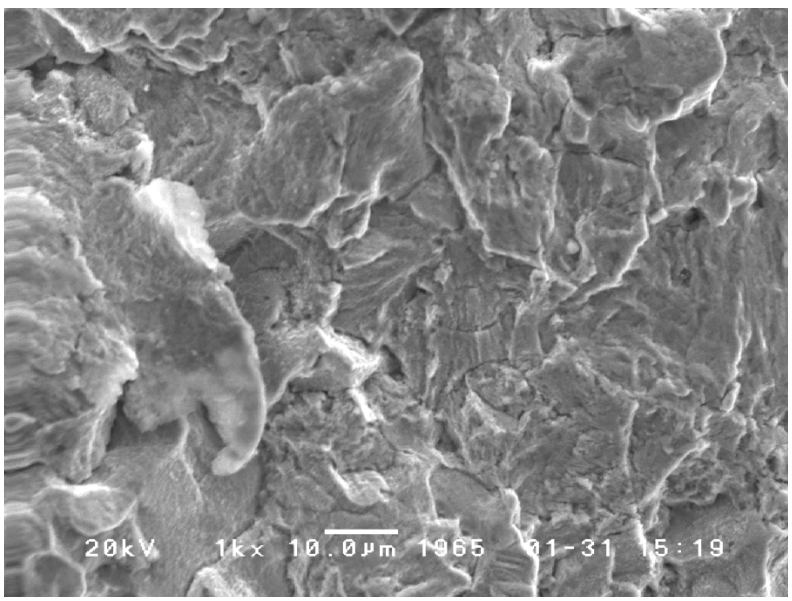

Figure 12 – SEM photomicrograph obtained at 1000X magnification at the center area indicating cleavage morphology

Fracture Summary:

The fracture examined occurred at the interface of a differential diameter section of the shaft and area of the smallest diameter of the loaded portion of the shaft. The abrupt nature of the diameter transition (lacking a transition radius and ultimately consisting of an undercut radius as subsequently described) is a likely surface stress riser. The fracture morphology is that of low stress but high stress concentration bending fatigue propagating uni-directional originating from the shaft surface at the diameter transition zone. Although final fracture did not occur, the retained metal portion is off center and likely indicates an axial bending component. Due to the nature of the failure mode, the fracture took time to propagate and ultimately fail. This observation is based on the differential oxidation rate observed in the brittle region of the failure.

Failures of these types are due to cycle bending overload of the material with some presence of bending or continuous loading exceeding the material engineered strength. The fracture is accelerated by a vibrational mode as well due to loosening or misalignment of the mating components.

Macro-etched shaft:

The transverse cross-section of shaft, which was finished on one side, was immersed in 1:1 HCl that was at a temperature of 170°F (77°C) for 45 minutes. It was then removed, washed with warm water, scrubbed with scotchbrite to remove the smut, and dried.

The etched surfaces were then rated according to the photo-macrographs of ASTM A604 as follows in table 1.

Table 1

Class	Condition	Severity Rating
1	Freckles	**A**
2	White Spots	**A**
3	Radial Segregation	**A**
4	Ring Pattern	**A**

The sample was not gassy. There was no flute cracks, butt tears, flake or splash. Please see Macro-image 13, which follows.

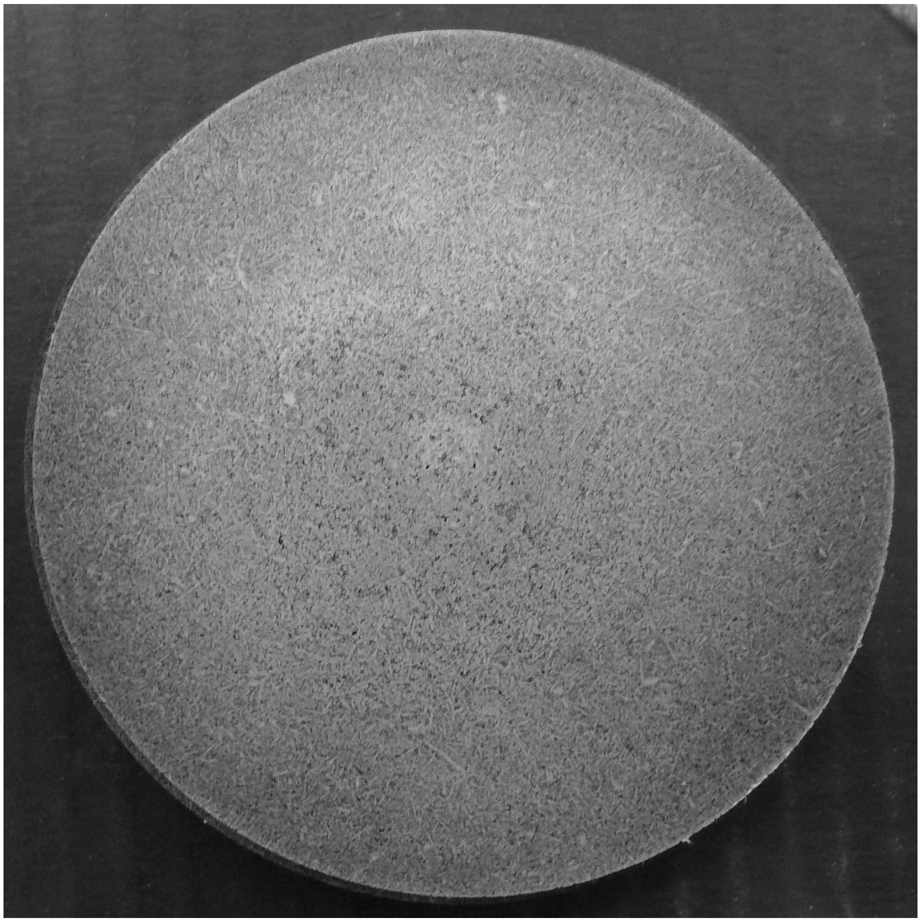

Etched condition. Figure 13 Reduced size.

Macro-image showing the macrostructure throughout cross-section.

Metallographic observations:

To further the investigation of the portion of the failed shaft was sectioned longitudinally (with respect to the axis of the part) throughout fractured region, metallographically prepared in accordance with ASTM E3-11, and microscopically examined in the as-polished and etched conditions.

Metallographic examination of the as polished longitudinal cross-section revealed numerous non-metallic inclusions throughout the matrix, which was rated at 100x for inclusion content of the steel by comparing with ASTM E45-10 ^{e1}, method A,
Plate I. (see fig.14)

Worst-Field Inclusion Ratings (Method A) Severity Levels

Classification of the inclusions	A (Sulfide Type)		B (Alumina Type)		C (Silica Type)		D (Globular Type Oxide)	
	Thin Series	Heavy Series	Thin Series	Heavy Series	Thin Series	Heavy Series	Thin Series	Heavy Series
Analyzed sample	2½	1	1½	1	½	½	1	½

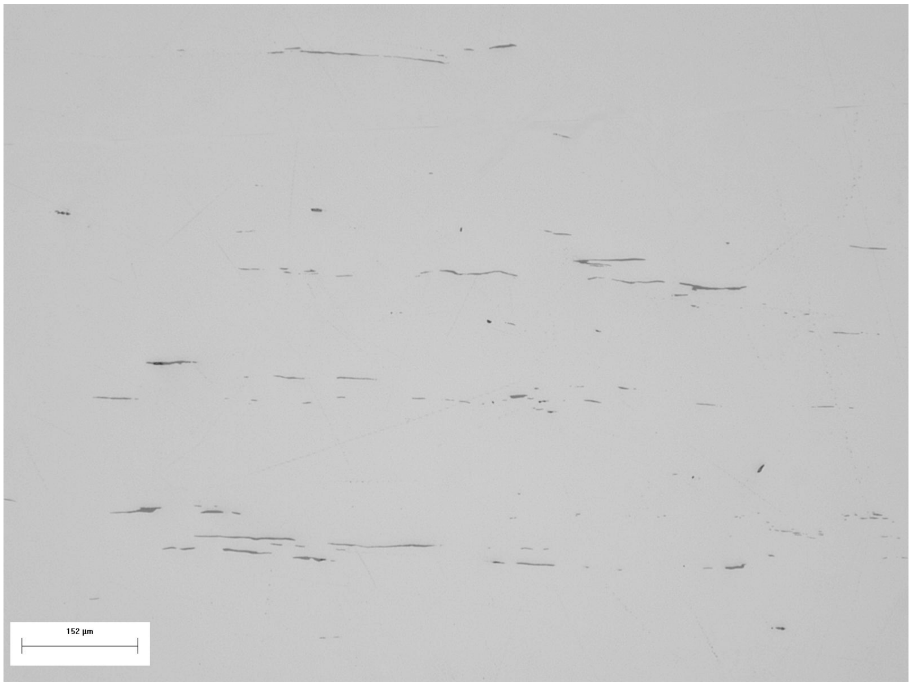

Figure: 14

Magnification: 100X

Condition: As-Polished

Comments: Micro-image of representative structure.

Metallographic examination of the etched cross-section under a low power microscope, revealed presence of the undercut at the sharp machined radius. The trans-granular crack originated from the step in undercut (see fig.15 red arrow) and progressed inward. Metallographic examination of the etched cross-section at higher-magnification revealed banded microstructure, which consists of continuous bands of fine lamellar pearlitic colonies in the ferritic matrix. (see fig.16) The average equiaxed ferritic grain size was estimated to be 7.0 in the section examined as rated to ASTM E112-10.

It should be noted that the high concentrations of non-metallic inclusions in the matrix and banded microstructure will decreases fatigue life of the material under cycle loading.

REMAINDER OF THIS PAGE INTENTIONALLY LEFT BLANK

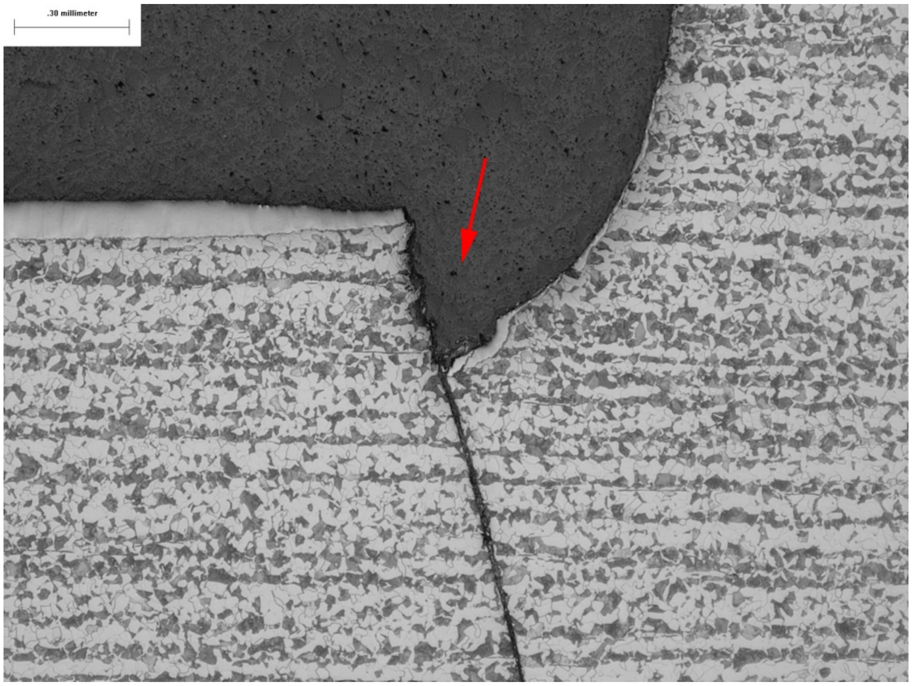

Figure: 15

Magnification: 50X

Condition: Etched with Nital

Comments: Micro-image illustrates undercut at the small machined radius and crack origin.

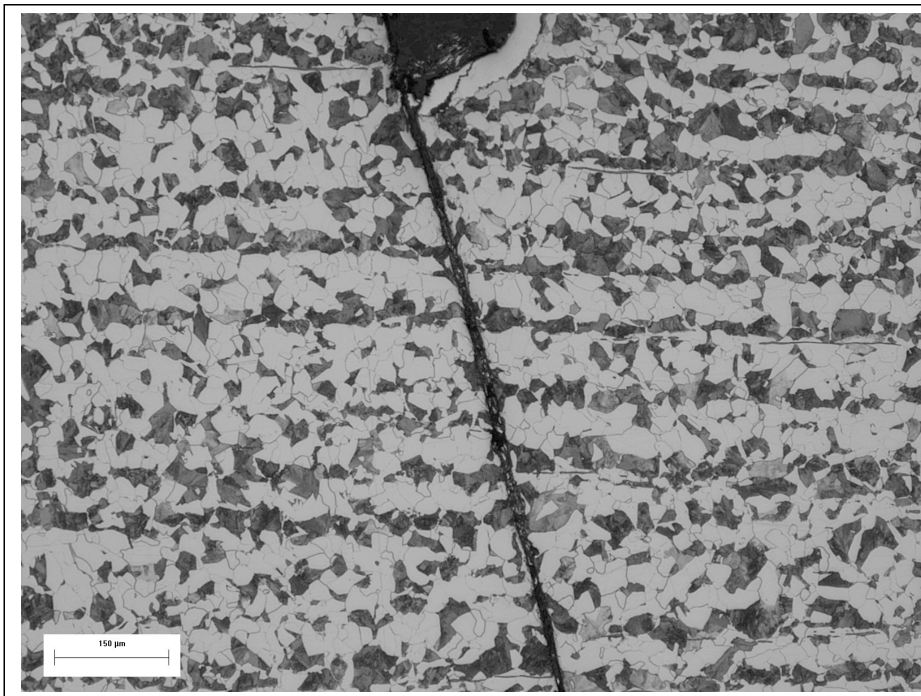

Figure: 16

Magnification: 100X

Condition: Etched with Nital

Comments: Micro-image of representative structure.

Hardness test:

Analytical method: ASTM E10.

Testing was performed on a polished cross-section of the shaft at locations specified in the figure below.

Location	BHN*
1	167
2	167
3	167
4	167
5	167
6	163
7	167
8	163
9	156

* Brinell hardness was performed with a 3000kg load and a Ø 10mm tungsten ball.

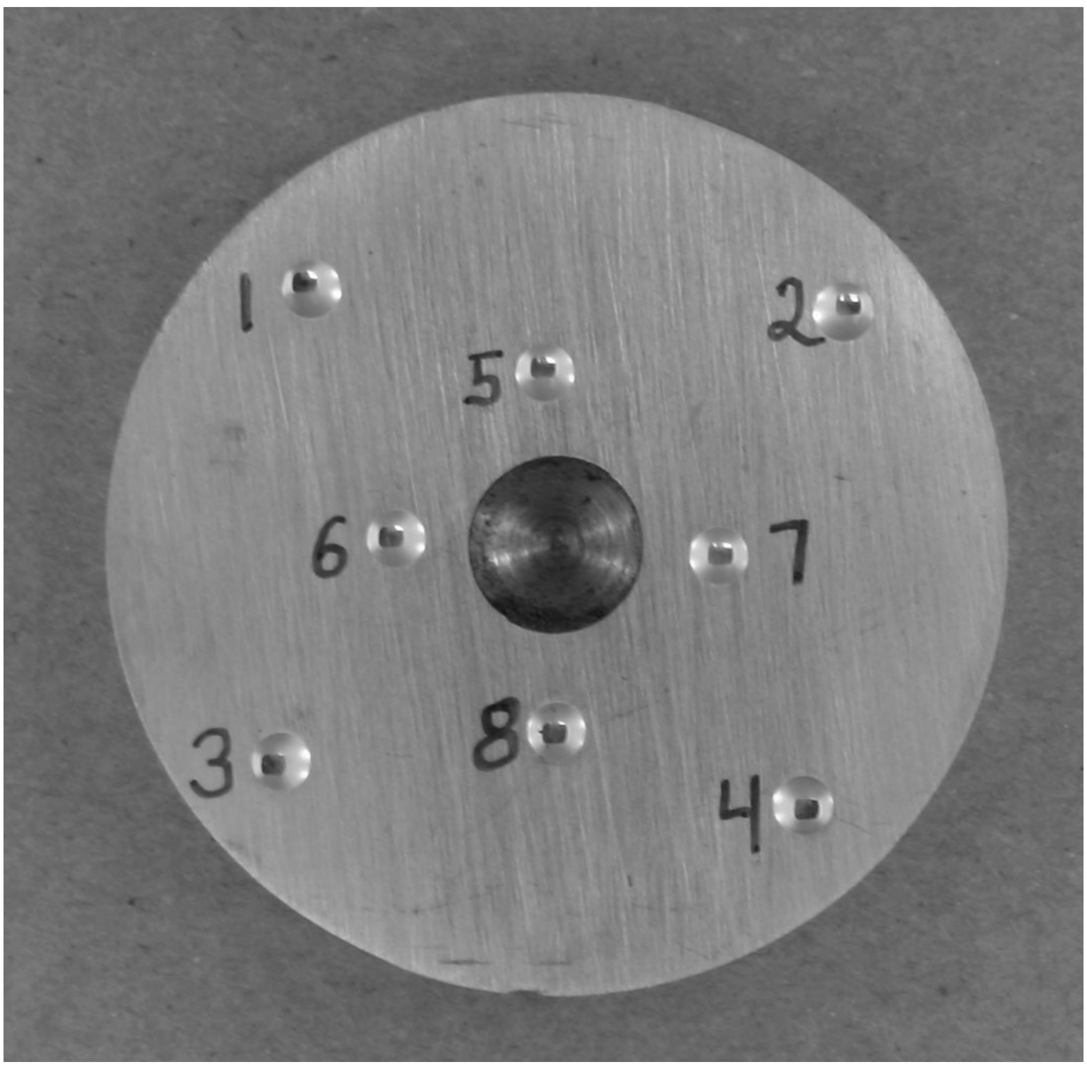

Figure 17 – Brinell hardness locations

Mechanical Properties:

Analytical method: ASTM A370, E8.

Specimens were extracted in the longitudinal direction from the shaft and prepared according to ASTM A370.

Test	Longitudinal specimen obtained at mid-radius
Tensile Strength	82.2ksi (559Mpa)
Yield Strength (0.2% Offset)	47.0ksi (319Mpa)
Elongation	29.9%

Chemical Analysis:

Analytical method:

1. ASTM E1019-03: Determination of Carbon, Sulfur, Nitrogen and Oxygen in Steel and Iron, Nickel, and Cobalt Alloys.
2. ISO1: Bulk chemical analysis by Glow Discharge- Optical Emission Spectrometry (GD-OES) in general accordance with ISO 14707:2000E First edition (2000-08-15).

Designation	Elements (All units are % by wt.)										
	C	S	P	Si	Mn	Cr	Ni	Mo	Ti	Al	Cu
Shaft section	0.14	0.025	0.018	0.25	1.15	1.03	0.17	<0.02	0.009	0.028	0.21
16MnCr5 specification	0.14-0.18	0.035 Max	0.025 Max	0.40 Max	1.0-1.3	0.8-1.1	NR	NR	NR	NR	NR

Physical and Chemical Properties Observations:

Based on the provided analysis, the material supplied for the shaft meets the chemical properties specification for 16MnCr5. The tensile and hardness properties are generally consistent throughout and are typical for the material in the normalized condition lacking any surface or core hardening. Macro and micro structure analysis indicates a banded structure of alternating ferrite and pearlite which would be undesirable for hardening. Micro structure analysis also indicates fairly heavy inclusion content, however lacking any specification for material cleanliness, the material meets the chemical requirements for the constituents.

Conclusion:

Based on the provided analysis and observations, the shaft failed due to bending fatigue and overload at the smallest cross-sectional area and area of highest surface energy (area transition with undercut transition radius). The failure propagated from the exterior circumference to the interior unidirectionally under bending overload and unbalanced loading. Analysis of the material properties as supplied indicates undesirable structure, however the material meets the specification as supplied in the normalized condition.

The failure of the shaft most likely occurred due to loading exceeding the engineered strength of the material and design.